Tracing Carbon and Nitrogen Microbial Assimilation in Suspended Particles in Freshwaters

Leonardo Mena-Rivera
University of Bristol
Charlotte E.M. Lloyd
University of Bristol
Michaela K. Reay
University of Bristol
Tim Goodall
Centre for Ecology and Hydrology, Wallingford
Daniel S Read
Centre for Ecology and Hydrology, Wallingford
Penny Johnes
University of Bristol
Professor Richard Evershed (r.p.evershed@bristol.ac.uk)
University of Bristol https://orcid.org/0000-0002-9483-2750

Research Article

Keywords: Amino acids, Dissolved organic matter, Nitrate, Particulate organic matter, Stable isotope probing, Suspended particles

Posted Date: October 29th, 2021

DOI: https://doi.org/10.21203/rs.3.rs-995821/v1

Version of Record: A version of this preprint was published at Biogeochemistry on April 5th, 2022. See the published version at https://doi.org/10.1007/s10533-022-00915-x.

Tracing carbon and nitrogen microbial assimilation in suspended particles in freshwaters

Leonardo Mena-Rivera[1,2], Charlotte E.M. Lloyd[1], Michaela K. Reay[1], Tim Goodall[3], Daniel S. Read[3], Penny J. Johnes[4], Richard P. Evershed[1]*

[1]Organic Geochemistry Unit, School of Chemistry, University of Bristol, Cantock's Close, Bristol BS8 1TS, UK

[2]School of Chemistry, Universidad Nacional, Heredia 86-3000, Costa Rica

[3]UK Centre for Ecology & Hydrology (UKCEH), Wallingford, Oxfordshire OX10 8BB, UK

[4]School of Geographical Sciences, University of Bristol, University Road, Bristol BS8 1SS, UK

*Corresponding author: r.p.evershed@bristol.ac.uk

Summary

Abstract: 193 words

Keywords: 6

Words: 6496 (excluding references)

Tables: 1

Figures: 6

References: 89

Supplementary information: 3 tables and 2 figures

Abstract

The dynamic interactions between dissolved organic matter (DOM) and particulate organic matter (POM) are central in nutrient cycling in freshwater ecosystems. However, the molecular-level mechanisms of such interactions are still poorly defined. Here, we study spatial differences in the chemical and molecular composition of suspended sediments in the River Chew, UK. We then applied a compound-specific stable isotope probing (SIP) approach to test the potential assimilation of ^{13}C,^{15}N-glutamate (Glu) and ^{15}N-nitrate into proteinaceous biomass by particle-associated microbial communities over a 72-h period. Our results demonstrate that the composition of suspended sediments is strongly influenced by the effluent of sewage treatment works (STW). Fluxes and percentages of assimilation of both isotopically labelled substrates into individual proteinaceous amino acids (AAs) showed contrasting dynamics in processing at each site linked to primary biosynthetic metabolic pathways. Preferential assimilation of the organic molecule glutamate and evidence of its direct assimilation into newly synthesised biomass was obtained. Our approach provides quantitative molecular information on the mechanisms by which low molecular weight DOM is mineralised in the water column compared to an inorganic substrate. This is paramount for better understanding the processing and fate of organic matter in aquatic ecosystems.

Keywords

Amino acids; Dissolved organic matter; Nitrate; Particulate organic matter; Stable isotope probing; Suspended particles

1. Introduction

The importance of organic matter in inland waters as nutrient and energy source for aquatic organisms (Yates et al. 2016; Mackay et al. 2020; Glibert et al. 2021), in controlling light attenuation (Mayer et al. 2006; Lu et al. 2013), and regulating the transport and bioavailability of pollutants (Artifon et al. 2018) and metals (Yamashita and Jaffé 2008) is widely acknowledged. A significant amount of organic matter in freshwater is processed in transit to coastal areas, preserved in soils and sediments or degraded by microorganisms (Brailsford et al. 2019b, a). Organic matter partially contributes to the burial of 0.6 Pg of C yr^{-1} in riverine sediments (Regnier et al. 2013) and to the evasion of 3.9 Pg of C yr^{-1} as CO_2 to the atmosphere (Drake et al. 2018), an amount equivalent to ~35% of the total anthropogenic CO_2 emissions. There is growing evidence that the current climate conditions and ever-increasing anthropogenic pressure are driving an increase in the concentration of organic matter in freshwaters (Evans et al. 2005; Monteith et al. 2007; Noacco et al. 2019). In this context, understanding the mechanisms in which organic matter, and related compounds, are processed across the landscape and within waterbodies is important to predict the potential impacts on the structure and functioning of the aquatic ecosystem.

Organic matter is typically classified as either dissolved (DOM) or particulate organic matter (POM) based on particle size with boundaries ranging from 0.2 to 0.7 µm. Although both phases exhibit different physical, chemical, and biological properties, they are actively linked to each other through several abiotic and biotic processes strongly influenced by environmental conditions (He et al. 2016; Einarsdóttir et al. 2020) including the degree of nutrient enrichment in the waterbody (Brailsford et al. 2019a). Leaching and physical abrasion of POM contributes to the DOM pool (Yoshimura et al. 2010) while DOM can form POM via a

range of physico-chemical processes including aggregation (Kerner et al. 2003), co-precipitation (Du et al. 2018) or selective sorption onto mineral surfaces (Aufdenkampe et al. 2001; Groeneveld et al. 2020). However, the processing of DOM is mainly regulated by living POM, whereby free-living and particle-associated microbial communities (Zeglin 2015; Mansour et al. 2018; Gweon et al. 2021) are central to the uptake of DOM into microbial organisms and primary producers, and its transfer to higher trophic levels.

Notably, particle-attached microbial communities are considered more active than their free-living counterparts (Crump et al. 1998; Smith et al. 2013). Suspended particles offer better ecological conditions, such as light exposure and availability to nutrients, which enhance co-existence of microorganisms and population diversity (Nemergut et al. 2013). Particle-attached microorganisms are therefore in a dynamic equilibrium with dissolved compounds, from which they can uptake nutrients. These biotic interactions that occur in the water column likely play a central role in nutrient cycling (Simon et al. 2002; Amalfitano et al. 2017; Glibert et al. 2021). Recently, Attermeyer et al. (2018) suggested that the partial loss of dissolved organic carbon (DOC) in rivers is due to remineralisation by suspended particle-attached microbes. Moreover, Jia et al. (2016) and Xia et al. (2017) showed that suspended particles impact nitrification and denitrification processes, expanding their significance to the processing of inorganic compounds (e.g., nitrate). It has been also demonstrated that particle-attached microorganisms respond to changes in nitrogen availability by potentially increasing assimilation (Bunch and Bernot 2012). Nevertheless, the molecular-level mechanisms by which these processes occur remain poorly defined.

Molecular-level and/or organism-specific processes can be elucidated through the application of stable isotope probing (SIP) techniques. SIP can provide metabolic and/or quantitative

85 information relating to how a given isotopically enriched substrate is utilised by a complex
86 microbial population. This is possible through the molecular analysis of labelled nucleic acids
87 (DNA/RNA-SIP) (Manefield et al. 2002; Chen and Murrell 2010), the interpretation of images
88 of biological samples via nano scale secondary ion mass spectroscopy (nanoSIMS) (Berthelot
89 et al. 2019; Dekas et al. 2019) and Raman spectroscopy (Wang et al. 2016) or the isotopic
90 analysis of specific biomarkers using gas chromatography-combustion-isotope ratio mass
91 spectrometry (GC-C-IRMS) (Bull et al. 2000; Evershed et al. 2006). The latter has been
92 successfully applied to study the incorporation of relevant substrates into microbial biomass
93 in soils (Knowles et al. 2010; Charteris et al. 2016; Reay et al. 2019) and riverine benthic
94 sediments (Veuger et al. 2005). Although stable isotopes have been widely used to study
95 different biogeochemical processes in aquatic ecosystems (reviewed by Sánchez-Carrillo and
96 Álvarez-Cobelas (2018)), most findings have relied on bulk isotopic measurements which
97 limits the disentangling of molecular-level mechanisms.

98 Herein, we sought to investigate the mechanisms in which living suspended POM act as a hot
99 spot for the processing of DOM and related compounds in a riverine ecosystem. We first
100 studied the chemical and molecular composition of suspended particles collected at three
101 contrasting sites in the River Chew, UK. We then conducted a SIP experiment where
102 suspended particles were separately incubated with two isotopically enriched substrates
103 under stable conditions. We used *L*-glutamic acid (^{13}C,^{15}N-Glu), a low molecular weight
104 compound central in amino acid (AA) biosynthesis, and potassium nitrate (^{15}N) that is one of
105 the major nitrogen containing compounds in rivers and a pollutant of concern. We
106 hypothesised that organic and inorganic compounds, containing carbon and/or nitrogen, are
107 partially assimilated into microbial biomass in the water column. We predicted enrichment in
108 the isotopic composition of C and/or N of individual proteinaceous AAs, which can be

109 determined via GC-C-IRMS. The rate and magnitude of such enrichments would provide
110 information on the biochemical pathways by which the substrates are assimilated by the
111 microbial communities.

112 **2. Materials and methods**

113 **2.1 Study site and sampling**

114 River Chew is a lowland river located in Bath and Northeast Somerset, United Kingdom. It
115 flows from Chew Valley Lake, south-west of Bath, to the north- east, where it discharges into
116 the Bristol Avon near the town of Keynsham, which then flows west to the Bristol Channel.
117 The catchment covers an area of 143 km^2. Discharge in the River Chew is highly influenced by
118 the regime of water release from Chew Valley Lake, a man-made reservoir that supplies
119 drinking water to the city of Bristol, as well as effluent discharges from a sewage treatment
120 works (STW). The study area is designated as Special Protection Area (SPA) and Site of Special
121 Scientific Interest (SSSI).

122 Samples were collected from three contrasting sites in the upper River Chew tributary (Fig.
123 S1). These were located downstream of the reservoir (S1), at the effluent discharge point
124 from the STW (S2), and downstream from the STW discharge (S3) where the stream was fully
125 mixed under baseflow conditions. The treatment methods at the STW comprises a) removal
126 of large materials, b) a primary settlement stage for further reduction of particle load, c)
127 biological filters (mixture of stone and plastic media) for breakdown of organic matter,
128 followed by a humus settlement tank, and d) aerated tertiary sand filters for phosphorus
129 removal. The STW discharge accounts for 20-50% of the total stream discharge. Samples of
130 suspended POM were collected from September to October 2018 using time-integrated
131 sediment samplers (Phillips et al. 2000) placed at 60% depth in the water column on a fixed

132 frame. Weekly routine checks were carried out to minimise inlet and outlet clogging. The
133 devices were sealed in the field and transported to the laboratory within 2 h. The sediments
134 were extracted from each device and stored at 4 °C in in situ river water until further
135 experiments; sub-samples were also stored at -70 °C. In addition, 2 L of river water was
136 extracted from each sampler, filtered using 0.5 µm pre-combusted (450 °C, 4 h) glass fibre
137 filters (Advantec® GC-50, Japan) and stored at -20 °C.

138 **2.2 Bulk measurements and nutrient analysis**

139 Total carbon (TC) and total nitrogen (TN) of suspended sediments were measured using a
140 Thermo EA1110 elemental analyser (MA, USA). Bulk ^{13}C and ^{15}N isotopic measurements were
141 determined using a Flash EA1112 Series NC Analyser coupled to a Thermo Finnigan DeltaPlus
142 XP (MA, USA). Inorganic nutrient analyses on filtered river water were conducted using a
143 Skalar San^{++} multi-channel continuous flow analyser (Breda, The Netherlands) following the
144 procedures outline by Yates et al. (2019). Nitrite (NO_2-N) was determined colourimetrically
145 at 540 nm after the reaction with *N*-(1-naphthyl)ethylenediamine dihydrochloride. Total
146 oxidised nitrogen (TON = NO_2-N + NO_3-N) was measured using the same principle as nitrite
147 analysis after nitrate reduction by hydrazinium sulfate. Nitrate concentrations were
148 calculated by subtraction of NO_2-N from TON. Total ammonium (NH_3-N + NH_4-N) analysis was
149 based on the modified Berthelot reaction and measured at 660 nm. Soluble reactive
150 phosphorus (PO_4-P) was determined using the molybdate/ascorbic acid blue method and
151 measured at 880 nm.

152 **2.3 Microbial community analysis**

153 DNA was extracted from suspended sediments using a PowerSoil® DNA Isolation Kit according
154 to the manufacturer's instructions. Bacterial amplicons were generated using a 2-step

amplification approach, with Illumina Nextera tagged primers: 16S rRNA (V4-V5 region) 515F GTGYCAGCMGCCGCGGTAA and 806R GGACTACNVGGGTWTCTAAT (Walters et al. 2016), each modified at 5' end with the addition of Illumina pre-adapter and Nextera sequencing primer sequences. Amplicons were generated using a high-fidelity DNA polymerase (Q5 Taq, New England Biolabs). After an initial denaturation at 95 °C for 2 min PCR conditions were: denaturation at 95 °C for 15 s; annealing at 50 °C. Annealing times were 30 s with extension at 72 °C for 30 s; repeated for 30 cycles. A final extension of 10 min at 72 °C was included. PCR products were purified using Zymo ZR-96 DNA Clean-up Kit following the manufacturer's instructions. MiSeq adapters and 8nt dual-indexing barcode sequences were added during a second step of PCR amplification. After an initial denaturation 95 °C for 2 min, PCR conditions were: denaturation at 95 °C for 15 s; annealing at 55 °C. Annealing times were 30 s with extension at 72 °C for 30 s; repeated for 8 cycles with a final extension of 10 min at 72 °C. Amplicon sizes were determined using an Agilent 2200 TapeStation system. Libraries were normalized using SequalPrep Normalization Plate Kit (Thermo Fisher Scientific) and quantified using Qubit dsDNA HS kit (Thermo Fisher Scientific). Each amplicon's pooled library was diluted to achieve 400 pM with 7.5% Illunina PhiX. Denaturation of each library was achieved with addition of 10% final volume of 2 M NaOH for 5 minutes followed by neutralisation with an equal volume of 2 M HCl. The libraries were then diluted to their load concentrations with Illumina HT1 Buffer. A final denaturation was performed by heating the libraries to 96 °C for 2 min followed by cooling in crushed ice. Sequencing of each amplicon library was performed on Illumina MiSeq using V3 600 cycle reagents.

176 **2.4 SIP experiment**

177 Mesocosms consisted of 300 mg of suspended sediments (wet weight) in 450 mL of in situ
178 sterilised-filtered river water. The latter was re-filtered and autoclaved (121 °C, 15 psi, 30 min)
179 the day of the experiment to sterilise. In situ river water was used in the mesocosms to keep
180 experimental and natural nutrient concentrations as similar as possible, given the known
181 impact of nutrient enrichment on organic matter processing in streams. Experiments were
182 conducted in 1 L pre-combusted Duran® bottles (450 °C, 4 h) at 19 °C and under artificial light;
183 constant-gentle stirring was applied to minimise sedimentation. An overnight acclimatisation
184 period was allowed prior substrate addition. Incubations were started after the addition of
185 100 µL of 25 mM *L*-glutamic acid ($x(^{13}C)$ = 99 %, $x(^{15}N$ = 99 %); Sigma Aldrich) or 100 µL of 320
186 mM KNO_3 ($x(^{15}N)$ = 10 %; Sigma Aldrich). Isotopes were added to increase the $\delta^{15}N$-value in
187 the river water $\sim$10000 ‰, which resulted in an increase of $\sim$1 mg/L N. Each mesocosm
188 was sampled twice (2 x 50 mL) after 3, 24, 48 and 72 h. Aliquots were immediately filtered
189 using 0.5 µm pre-combusted (450 °C, 4 h) glass fibre filters (Advantec® GC-50, Japan); the
190 latter were rinsed twice with double distilled water to remove the excess of substrate. Both
191 fractions sampled (sediments and filtered river water) were then stored at -20 °C.

192 **2.5 Total hydrolysable amino acids**

193 Analysis of total hydrolysable amino acids (THAAs) were performed following Charteris et al.
194 (2016). In brief, freeze-dried sediments ($\sim$10 mg) were hydrolysed with 5 mL of 6 M HCl at
195 100 °C for 24 h under N_2. An internal standard (norleucine, 1000 µg mL^{-1}) was added before
196 hydrolysis. Hydrolysates were separated by centrifugation, dried under N_2 at 60 °C and stored
197 in 0.1 M HCl at -20 °C until further analysis. AA were isolated by cation-exchange column
198 chromatography (Dowex® 50WX8) and converted into their *N*-acetyl, *O*-isopropyl derivatives

199 with acetyl chloride, trimethylamine, and acetic anhydride. Derivatives were then quantified
200 by conventional gas chromatography (GC-FID) (Agilent Technologies 7890B, CA, USA). The
201 system was fitted with a DB-35 column (35 %-phenyl-methylpolysiloxane, mid-polarity, 30 m
202 x 0.32 mm inner diameter, film 0.5 µm). The carrier gas was He at 2 mL min^{-1} and the GC
203 operated under constant flow. The temperature programme used was: 70 °C (2 min) to 150
204 °C at 15 °C min^{-1}, then to 210 °C at 2 °C min^{-1}, then to 270 °C (10 min) at 8 °C min^{-1}.
205 Quantification was estimated based on the internal standard method and individual response
206 factors for each AA.

207 **2.6 GC-C-IRMS analysis**

208 The ^{13}C and ^{15}N values of the individual derivatised AAs were determined via GC-C-IRMS. ^{15}N
209 measurements were performed using a Thermo Finnigan Trace 2000 GC (Milan, Italy) coupled
210 with a Thermo Finnigan DeltaPlus XP IRMS (Bremen, Germany) via a GC Combustion III
211 interface. The GC was fitted with a DB-35 column (35 %-phenyl-methylpolysiloxane, mid-
212 polarity, 30 m x 0.32 mm inner diameter, film 0.5 µm). The temperature programme was: 40
213 °C (5 min) to 120 °C at 15 °C min^{-1}, then to 180 °C at 3 °C min^{-1}, then to 210 °C at 1.5 °C min^{-1},
214 then to 270 °C (1 min) at 5 °C min^{-1}. The carrier gas was He at 1.4 mL min^{-1} and the GC operated
215 in constant flow mode. Individual derivatised AA were combusted at 1030 °C over Cu and Ni
216 wires. A cryogenic trap with liquid nitrogen was used to remove CO_2. The mass spectrometer
217 operated in EI mode at 124 eV and data acquisition included *m/z* 28, 29 and 30. Carbon
218 isotopic measurements were carried out using a Trace GC Ultra (Bremen, Germany) coupled
219 with a Thermo Finnigan Delta V (Bremen, Germany) IRMS. The GC operated under the same
220 conditions described for the ^{15}N measurements, except for the carrier gas flow which was set
221 up at 1 mL min^{-1}. The reactor temperature was 1000 °C. The mass spectrometer operated in

EI mode at 124 eV and data acquisition included *m/z* 44, 45 and 46. The original $\delta^{13}C$ value of each individual AA was determined after correction of its derivatised form (Docherty et al. 2001).

2.7 Data analysis

All data processing was performed in R version 4.1.0 (R Core Team 2021).

2.7.1 Bioinformatics

Each amplicon's Illumina demultiplexed sequences were processed using packages *ShortRead* (Morgan et al. 2009) and *Biostrings* (Pagès et al. 2021), along with cutadapt (Martin 2011) to search for and remove primers. Dada2 (Callahan et al. 2016) was used to filter, denoise and merge the sequences with following parameters: forward reads were trimmed to 250 and reverse to 200. Filtering settings were maximum number of Ns (maxN) = 0, maximum number of expected errors (maxEE) = (5,5). Sequences were de-replicated and the DADA2 core sequence variant inference algorithm applied. Forward and reverse reads were then merged using mergePairs function to produce Amplicon sequence variants (ASVs). Chimeric sequences were removed using removeBimeraDenovo at default settings and the sequence table constructed from the resultant ASVs. ASVs were subject to taxonomic assignment using assignTaxonomy function and the SILVA training database (Quast et al. 2013).

2.7.2 SIP calculations

Isotopic enrichments of individual AAs are reported as the normalised excess atom fraction following:

$$x^{E}({}^{i}E)_{N} = \frac{x({}^{i}E)_{P} - x({}^{i}E)_{c}}{x({}^{i}E)_{s}}$$

where $x^E({}^iE)_N$ is the normalised excess atom fraction of the isotope ${}^iE$ (^{13}C or ^{15}N) of an individual AA, $x({}^iE)$ is the atom fraction of the enriched isotope in that AA in the sample (*P*) or the control (*c*), and $x({}^iE)_s$ is the atom fraction of the isotope in the substrate corrected for any dilution effect due to background/ambient concentration. The atom fractions are calculated from the δ-value (Coplen 2011) following:

$$x({}^iE) = \frac{1}{1 + \frac{1}{(\delta^iE + 1)R({}^iE/{}^jE)_{std}}}$$

where $R({}^iE/{}^jE)_{std}$ is the heavy to light isotope ratio of internationally agreed standards. Stable isotope standards include the Vienna Pee DeeBelemnite (VPDB) (^{13}C/^{12}C =0.0112372) (Craig 1957) and air (^{15}N/^{14}N =0.0112372) (Junk and Svec 1958; Meija et al. 2016) for C and N determinations, respectively.

Specific assimilation (*V*) and transport rates (ρ) for each AA were calculated after 3 h (Dugdale and Goering 1967; Glibert et al. 2019). Enrichments are also reported as the percentage of assimilation, $A({}^iE)_{AA}$, into each individual AA derived from the added substrate (Knowles et al. 2010) following:

$$A({}^iE)_{AA} = \frac{mol^E({}^iE)_P}{mol({}^iE)_s} 100$$

where $mol^E({}^iE)_P$ is the total amount of the enriched isotope (^{13}C or ^{15}N) in the mesocosm, and $mol({}^iE)_s$ is the amount of that isotope added from the substrate. Negligible losses of the substrate over time are assumed.

2.7.3 Statistical analysis

Linear mixed-effects modelling was applied to evaluate the significance of sampling location, treatment, and incubation period (i.e., time) in explaining the variation of the concentration of THAAs, or individual AAs, during the SIP experiment. Sampling location, treatment, and time were set as fixed effects, and the mesocosms as random effect. Assumptions of normality and homoscedasticity were checked using standard diagnostics graphs. Final model selection was based on the Akaike Information Criterion (AIC). Models were run using the *nlme* package (Pinheiro et al. 2021).

Deming regression was applied to estimate the ^{13}C:^{15}N ratio of Glx (Glu + Gln) and Pro during the first 24 h of incubation; correlation coefficients were calculated using Spearman's rank correlation. Significant differences between the ^{13}C:^{15}N ratio of Glx and Pro were tested by contrasting the regression slopes using a *t*-test.

3. Results and discussion

3.1 Chemical composition

Significant changes in the chemical composition of the suspended particles in the River Chew, UK were observed between sites (Table 1). The impact of the STW effluent led to an increase in the concentration of TC, TN and THAAs. In addition, bulk $\delta^{15}N$ values showed enrichment (~3‰) at sites S2 and S3, which has been previously associated with human sewage pollution (Steffy and Kilham 2004; Costanzo et al. 2005). A total of 13 AAs were identified with concentrations ranging from 0.40 to 4.92 mg g^{-1} at site S1, from 0.76 to 12.04 mg g^{-1} at site S2, and from 0.14 to 4.73 mg g^{-1} at site S3. The contribution of the THAAs to the TC and to the TN accounted for >10% and >50%, respectively. The molecular composition of the pool of

283 THAAs, expressed as mol %, followed: Asx (Asp + Asn) > Gly > Ala > Thr > Ser > Glx > Leu > Val
284 > Pro > Lys > Phe > Hyp > Tyr. This overall composition agrees with previous studies where
285 the neutral, acidic and hydroxyl AAs were reported to be the most dominant (GUPTA et al.
286 1997; Fernandes et al. 2019, 2020). The high contribution of the THAAs to TN and the
287 relatively moderate abundance of Gly (∼14%) indicate the high bioavailability and low
288 diagenetic state of organic matter in the suspended sediments (Cowie and Hedges 1994;
289 Dauwe and Middelburg 1998). The significant decrease in the concentration of individual AAs
290 at site S3 might suggest a different source of suspended sediments; however, similarities in
291 the δ^{15}N values of individual AAs shows connectivity in the transport of suspended particles
292 between sites S2 and S3 (Table S1). Therefore, the composition of the suspended material at
293 site S3 appears to be a mixture of particles from the STW outfall with significant contribution
294 from the floodplains or bank erosion at this site.

295 **3.2 Microbial community composition**

296 Suspended sediments harbour complex and diverse microbial communities that play a crucial
297 role in the biogeochemical cycles. High throughput sequencing revealed changes in the
298 diversity and composition of the riverine microbial communities upstream and downstream
299 from the STW effluent discharge point. In total 147425 high-quality bacterial 16S rRNA gene
300 sequences were obtained and classified into 1111 ASVs. Both richness and diversity decreased
301 downstream from the STW effluent (Table 1). This phenomenon has been previously
302 observed in freshwaters receiving sewage effluents (Drury et al. 2013; Burdon et al. 2020).
303 Although treated and untreated sewage discharges led to an increase the bioavailability of
304 both dissolved organic and inorganic nitrogen and phosphorus in freshwaters (Yates et al.
305 2019) stimulating bacterioplankton growth, the discharge of potentially harmful compounds

306 that escape conventional treatment could explain the negative impact on microbial diversity
307 (Chonova et al. 2018; Hagberg et al. 2021). In the same study reach, Pemberton et al. (2020)
308 reported changes in the chemical composition of DOM due to STW effluent, highlighting the
309 presence of pharmaceuticals, illicit drugs, and flame retardants. Future studies are needed to
310 assess the impact of these pollutants on the structure and functioning of aquatic
311 microorganism communities. Despite this decrease in diversity, the three sampling sites
312 shared 159 ASVs which comprised for 55.7-64.0% of the total relative abundance. Adjacent
313 sites shared higher number of ASVs. For instance, site S1 and S2 shared 84 additional ASVs
314 (243 in total), whereas sites S2 and S3 shared 63 ASVs (222 in total).

315 The composition of the microbial communities associated to the suspended sediments was
316 dominated by *Proteobacteria* (55.3-59.5%) (Fig. 1); in particular, the class
317 *Gammaproteobacteria* was the most abundant as found in other riverine sediments (Wang
318 et al. 2018). In less abundant phyla were *Cyanobacteria* (6.3-8.2%), *Nitrospirota* (3.3-8.3%),
319 *Bacteroidota* (3.6-6%), and *Acidobacteriota* (4.2-5.9%). Among the three sites, the shared
320 ASVs included the phyla described in Fig. 1, together with *Desulfobacterota*, *NB1-j* and *RCP2-*
321 *54,* which were found in <1% of the relative abundance. Some spatial differences in microbial
322 composition were also observed. The relative abundance of *Proteobacteria* and *Nitrospirota*
323 increased downstream (>4%), whereas the relative abundance of *Bacteroidota* and
324 *Acidobacteriota* decreased (<3%). The phyla *WPS-2* and some classes such as *OLB14*, *TK10*,
325 *Babeliae*, *Gracilibacteria*, *Kapabacteria* and *Vampirivibrionia* were only found at sites S2 and
326 S3. The higher abundance of *Proteobacteria* downstream (sites S2 and S3) might be related
327 to the increase in the concentration of nutrients in the stream due to the STW effluent. This
328 is in line with previous studies showing a positive correlation between the abundance of
329 *Proteobacteria* and the availability of nutrients (Dai et al. 2013). Similarly, *Nitrospirota* are

abundant in STW and well known for catalysing the second step of nitrification (Wu et al. 2019); thus, their increased abundance may be a result of an increase in the concentration of ammonium in the stream. In general, the microbial composition mainly comprised heterotrophic organisms with the potential ability to degrade a broad range of organic molecules. Estimating the different fluxes in the processing of these organic compounds compared to inorganic compounds, at spatial and temporal scales, is key in biogeochemical cycling.

3.3 SIP experiment

3.3.1 THAAs concentration

The addition of the two isotopically enriched substrates had a negligible effect on the concentration of THAAs in the sediments during the SIP experiment. The results of the mixed effects model showed non-significant differences in the concentration of THAAs among treatments ($F(2,4) = 3.44$, $P = 0.135$). In contrast, there were significant effects of site ($F(2,4) = 74.78$, $P = 0.0007$) and time ($F(1,62) = 21.62$, $P < 0.0001$) (Fig. S2). The effect of site confirmed that the concentration of THAAs in the suspended sediments was significantly higher at site S2 in comparison to sites S1 and S3, as shown in Section 3.1. Despite the significant effect of time, the standard error and the confidence intervals of the means per site during the experiment were 1.38 and 7.7 mg g^{-1} (95% confidence level), respectively. Because one of the added substrates was Glu, the variation in the concentration of Glx was also tested. Similar results to the concentration of THAAs were obtained with significant effects of site ($F(2,4) = 37.59$, $P = 0.0026$) and time ($F(1,62) = 25.36$, $P < 0.0001$). The effect of treatment was also likely significant ($F(2,4) = 6.88$, $P = 0.0507$). However, the slightly higher concentrations of Glx were observed in the controls and not the treatments. These results

indicate that sorption processes of $^{13}C,^{15}N$-Glu onto the mineral phase or biomass on the particles were likely negligible. Therefore, it can be assumed that the $^{13}C,^{15}N$-Glu measured in excess was primarily taken up into microbial cells.

3.3.2 $^{13}C,^{15}N$-Glu treatment

Isotope values of individual AAs showed transfer of ^{13}C and ^{15}N from Glu into newly synthesised protein biomass. This isotopic enrichment was used to estimate specific assimilation rates (V, h^{-1}) for each AA. Assimilation rates of ^{15}N were higher than ^{13}C (Table S2). The assimilation of ^{15}N from Glu is expected to be faster as it participates in single-step transamination reactions in the synthesis of other AAs (Knowles et al. 2010). On the other hand, the assimilation of ^{13}C is mediated by glutamate dehydrogenase where Glu is deaminated to produce ammonia and 2-oxoglutarate. The latter is then incorporated into the citric acid cycle (TCA) (Miflin and Habash 2002; Feehily and Karatzas 2013). Lys and Asx showed the highest average assimilation rates for both isotopes; after excluding Glx. In contrast, Hyp and Leu showed the lowest average assimilation of ^{13}C and ^{15}N, respectively. It should be noted that the low concentration of Hyp and Tyr impeded determination of their ^{15}N contents.

A quantitative assessment of the assimilation of both isotopes, as given by the estimation of transport rates (nmol g^{-1} h^{-1}), showed higher assimilation of ^{13}C over ^{15}N, except for Gly (Table S3). The highest average values were presented in Asx, which is in close metabolic proximity to Glu, but also in high abundance. The higher transport of ^{15}N over ^{13}C into Gly during the first 3 h of incubation is particularly interesting as it might suggest that the main biosynthetic pathway of Gly was not dominant. Gly is primarily synthesised from Ser; in this pathway, 3-phosphoglycerate is oxidised to 3-phosphohydroxy-piruvate followed by the addition of an

amino group by a 3-phosphoserine aminotransferase to produce 3-phosphoserine. The latter is then hydrolysed to form Ser, which can be converted to Gly by serine hydroxymethyltransferase (Stauffer 2004). A significantly fast transamination reaction followed by the conversion of Ser to Gly could explain the higher assimilation of ^{15}N over ^{13}C. However, transport rates of ^{15}N into Ser do not fully support this as they were lower compared to the ones of Gly. Gly can also be synthesised from glyoxylate (Conley et al. 2017; Caspi et al. 2019). In this case, the transamination is mediated by alanine. If this pathway was dominant, it could explain the high incorporation of ^{15}N into Gly. The faster assimilation and high transport rates of ^{15}N into Ala versus Gly would support this hypothesis.

Based on the amount of substrate added, the percentage of assimilation of ^{15}N was higher than ^{13}C, except in Phe (Fig. 2). In most cases, the decoupling between both isotopes likely occurred after 3 h of incubation. However, this was not the case for Glx and Pro where the coupling was conserved up to 24 h after the substrate addition. Trends in assimilation were different among AAs, but they were likely linear during the first 24 h of the experiment. After this period, some AAs, such as Ala, Gly, Leu, and Phe, likely reached a plateau or showed an apparently decreasing trend. In contrast, Ser, Thr and Val showed an increasing trend of assimilation over the course of the experiment. Unlike the other AAs, Lys showed an exponential assimilation. After 72 h, average microbial assimilation of ^{13}C was dominated by Glx (*M* = 2.91%, *SE* = 0.13) and Asx (*M* = 2.22%, *SE* = 0.11) while the assimilation of ^{15}N was higher in Asx (*M* = 4.70%, *SE* = 0.22), Glx (*M* = 4.19%, *SE* = 0.22), Gly (*M* = 4.03%, *SE* = 0.32) and Ala (*M* = 3.92%, *SE* = 0.43). Microbial assimilation of Glx included in excess ^{13}C and ^{15}N.

To better understand the uncoupling of ^{13}C and ^{15}N, the ^{13}C:^{15}N ratio was estimated for all the individual AAs at each time point (Fig. 3A). Two maximum values were observed at ~2 and

399 ~5 after 3 h of incubation. As expected, the ratio shifted towards lower values over time. This
400 is likely due to the transfer of ^{13}C into the synthesis of non-proteinaceous compounds or its
401 release as CO_2; for instance, during the conversion of 2-oxoglutarate into succinyl-CoA. On
402 the other hand, the maximum C:N value of ~5 is close to the nominal C:N ratio of Glu. This
403 confirmed that mostly all the ^{13}C,^{15}N-Glu was transported directly into the microbial cells as
404 proposed in section 3.3.1. To evaluate whether Glu is directly utilised for the synthesis of
405 proteinaceous biomass, the C:N ratio of Glx and Pro were compared. The biosynthesis of Pro
406 involves the reduction of the γ-carboxyl group of Glu to produce γ-glutamic semialdehyde,
407 which spontaneously cyclises to *L*-Δ^1-pyrroline-5-carboxylate. This compound is then reduced
408 to produce Pro (Csonka and Leisinger 2007; Fichman et al. 2015). In this pathway, the C:N
409 ratio is conserved; therefore, it should be similar between the substrate (Glu) and the product
410 (Pro). The ratios for both AAs were estimated using a regression model over the first 24 h of
411 incubation (Fig. 3B and 3C). The concentrations of ^{13}C and ^{15}N were strongly correlated for
412 each AA during this period ($\rho > 0.986$, $P < 0.0001$). Estimated regression slopes were 4.656
413 ($SE = 0.321$) for Glx, and 4.735 ($SE = 0.207$) for Pro. Both values were not significantly different
414 between each other ($t(22) = 0.206$, $P = 0.8384$). An individual comparison against the nominal
415 C:N ratio of 5 showed non-significant difference for Glx ($t(11) = 1.072$, $P = 0.3066$) or Pro (t(11)
416 = 1.283, $P = 0.2260$). This shows that the direct uptake and assimilation could be the dominant
417 mechanism for C and N incorporation from AAs into microbial biomass in freshwaters.

418 **3.3.3 ^{15}N-nitrate treatment**

419 Specific assimilation rates (V, h^{-1}) for ^{15}N-nitrate were considerably lower than ^{15}N-Glu (Table
420 S2). This is because the assimilation of nitrate occurs via several biochemical reactions which
421 are more energy demanding. Nitrate must be first reduced to nitrite and then to ammonia by

nitrate and nitrite reductases, respectively (Stein and Klotz 2016; Zhang et al. 2020). Thereafter, either glutamate dehydrogenase or glutamine synthetase incorporate ammonia into biomass (Reitzer 2004). The highest average assimilation rates were found in Phe and Glx. Some AAs exhibited δ^{15}N values lower than the natural abundance after 3 h of incubation resulting in negative assimilation rates (Table S2). This was particularly apparent in Gly, Leu, Lys, Pro, Ser and Val at sampling site S3. Similar trends were seen by (Charteris et al. 2016) after the application of ^{15}N-nitrate to soil. Although the reason for this is unclear, the high energy requirements to assimilate nitrate could led to the assimilation of energy-dense N-containing compounds depleted in ^{15}N. Transport rates (nmol g^{-1} h^{-1}) of Glx, Asx and Ala presented the highest average values which agree with the metabolic proximity and the observed transport rates for assimilation of ^{15}N-Glu.

The percentages of assimilation of ^{15}N-nitrate over time followed a different pattern compared to the ^{15}N-Glu treatment. The trends were characterised by a steady assimilation during the first 24 h, followed by a significant increase towards the end of the experiment (Fig. 4). The delay in the assimilation of ^{15}N-nitrate, as observed in Fig. 4, could be related to the preferential assimilation of ammonia, due to high energy costs, and the inhibition of ammonia over the uptake and assimilation of nitrate (Dortch 1990; Glibert et al. 2016). Highest assimilation was found in Asx (*M* = 0.45%, *SE* = 0.18) and Glx (*M* = 0.42%, *SE* = 0.16) whereas the lowest were present in Phe (*M* = 0.066%, *SE* = 0.026) and Val (*M* = 0.134%, *SE* = 0.060). Assimilation at site S1 was significantly higher compared to the other sites.

3.3.4 Synthesis

The data presented here reveals pathways of carbon and nitrogen assimilation by particle-associated freshwater microbial communities. The rates and percentages of assimilation of

each AA from the three study sites were combined and linked to the primarily biosynthetic pathways to compare the fluxes and connectivity of ^{13}C and ^{15}N processing (Fig. 5). For simplification, the percentages of assimilation were normalised to the amount of ^{15}N-Glu added, which was also scaled to represent the total pool of Glx. Secondary biosynthetic pathways were not included. The diagrams show the average composition of the pool of THAAs in mol %. The fluxes and biosynthetic links are useful to understand the metabolism of the complex consortia of microorganisms, associated with suspended sediments, processing DOM and inorganic substrates in the water column. It must be noted that the rates of assimilation presented here should be interpreted with caution and not be considered 'real' rates. The concentration of suspended sediments added to the mesocosms exceeded the ambient concentration in the stream at the time of sampling but was below the global average (Müller et al. 2021). Moreover, the addition of ^{13}C,^{15}N-Glu at tracer level (<10%) was not possible; but the amount added was not higher than 10% of the TN in the mesocosm. Nevertheless, it was shown that the addition of the substrates did not enhance microbial biomass production (section 3.3.1).

As previously discussed, there were significant differences in the total assimilation of ^{13}C-Glu and ^{15}N-Glu ($^{15}N > ^{13}C$) and a preference of ^{15}N from the organic versus the inorganic (^{15}N-Glu > ^{15}N-nitrate) substrate. Overall, the total microbial assimilation into newly synthesised proteinaceous biomass was estimated at 11.95% (*SE* = 0.56) and 27.60% (*SE* = 1.10) of ^{13}C and ^{15}N from Glu, respectively; and 3.18% (*SE* = 1.30) of ^{15}N from nitrate (Fig. 6A). Spatial differences in the total percentage of assimilation were also observed (Fig. 6B). There were likely higher percentages at site S2 and S3 for the ^{13}C,^{15}N-Glu treatment, and at site S1 for the ^{15}N-nitrate treatment (Fig. 5B). These percentages were estimated after excluding the ^{13}C,^{15}N-Glu in excess and after 72 h of incubation. However, the maximum levels of assimilation were

reached at different times at each site (Fig. 2 and 4); in particular, assimilation of ^{15}N-nitrate did not reach a plateau before the end of the incubation.

Similar spatial differences were also observed in the assimilation and transport rates (Table S2 and S3). For the ^{13}C,^{15}N-Glu treatment, assimilation rates were slightly higher at site S1 in comparison to S2, and lower at S2 in comparison to S3. In decreasing order, they followed sites S3 > S1 > S2. In contrast, transport rates were higher at site S2, probably due to the higher concentration of biomass, followed by sites S3 and S1. For the ^{15}N-nitrate treatment, a different trend was observed with higher assimilation and transport rates at site S2, followed by sites S1 and S3. These contrasts are based on cumulative values but not all the individual AAs followed the same trends. It was also observed that the decreasing order of the assimilation rates of individual AAs was different among sites suggesting distinctive processing of the substrates. In this regard, the experimental approach was affected by restricted replication which hindered a robust spatial comparison of the fluxes and percentages of assimilation. Therefore, discussion of the metabolic pathways at each site is not included in this study. The trends of the percentages of assimilation over the course of experiment were also likely different (Fig. 2 and 4). There was a more rapid assimilation at site S1 during the first 24 h compared to the other two sites. This was particularly emphasised in the ^{15}N-nitrate treatment (Fig. 4). Such differences could be influenced by the changes in the availability of nutrients at each site (i.e., ambient concentrations) as well as differences in microbial community composition (Middelburg and Nieuwenhuize 2000). For instance, the concentration of N-containing compounds (e.g., NH_4^+ and NO_3^-) increased downstream due to the STW outfall. Regarding the changes in the microbial composition, our approach does not allow establishing direct links between structure and functioning. However, it does provide evidence of the complexity of the population, and an overall representation

493 (mechanistic and quantitative) of how the substrates are processed. Future efforts could be
494 oriented to a) the better understanding of the spatial and temporal differences in rates and
495 fluxes of assimilation for each AA, and b) application of quantitative functional genomics in
496 combination with SIP techniques.

497 **4. Conclusions**

498 The chemical and molecular characterisation of the sites, in combination with the application
499 of compound-specific SIP, provided insights into the role of suspended POM in freshwater
500 nutrient cycling. In particular:

501 a. Regardless the close proximity of the study sites, the composition of suspended
502 sediments in the River Chew appeared to be distinct and highly influenced by the
503 effluent of the STW.

504 b. Compound-specific isotope analysis of individual AAs allowed demonstration of
505 assimilation of glutamate and nitrate into microbial biomass. Specific assimilation and
506 transport rates showed preference for the organic vs the inorganic substrate and
507 provided insights into the biochemical pathways by which the substrates are
508 assimilated by the microbial communities.

509 c. Dual isotope analysis (^{13}C and ^{15}N) of Glx (glutamate and glutamine) and proline
510 unequivocally confirmed the coupled assimilation of C and N into proteinaceous
511 biomass suggesting that the direct uptake and assimilation of Glu could be the
512 dominant mechanisms regarding its processing.

513 d. The fluxes of assimilation of the substrates into the THAAs pool varied spatially, which
514 may be related to the distinct physical, chemical, and biological conditions at each site.

515 Our results highlight the value of SIP techniques to elucidate the fate of organic and inorganic
516 compounds in freshwaters. This is particularly relevant for the better understanding of the
517 molecular mechanisms regarding processing of low molecular weight DOM in freshwater
518 ecosystems and the impacts of DOM and POM of differing molecular composition on the
519 freshwater biota.

520 **Acknowledgements**

521 We thank the UKRI National Environmental Isotope Facility at the School of Chemistry,
522 University of Bristol for analytical support. We also thank Boris Banecki and Jonathan
523 Pemberton for their assistance during sampling, and Alison Kuhl and Catherine Bayliss for
524 their collaboration with isotope and nutrient analyses, respectively.

525 **Authors' contributions**

526 LM-R and RPE designed the research. PJJ advised on the design of the sampling programme
527 and the nutrient chemistry analyses. LM-R, CEML and TG performed the experiments; LM-R
528 and TG analysed the data with input from MKR and DSR. LM-R wrote the paper with
529 contributions of all authors.

530 **Funding**

531 This work was partly developed under the DOMAINE programme (Characterisation of the
532 nature, origins, and ecological significance of dissolved organic matter in freshwater
533 ecosystems) which was supported by the Natural Environment Research Council, UK
534 (NE/K010689/1 to PJJ and RPE). LM-R was funded by Universidad Nacional, Costa Rica.

535 **Conflict of interest**

536 The authors declare no conflict of interest.

Data availability

The datasets generated during the current study are available from the corresponding author on reasonable request.

References

Amalfitano S, Corno G, Eckert E, et al (2017) Tracing particulate matter and associated microorganisms in freshwaters. Hydrobiologia 800:145–154. https://doi.org/10.1007/s10750-017-3260-x

Artifon V, Zanardi-Lamardo E, Fillmann G (2018) Aquatic organic matter: Classification and interaction with organic microcontaminants. Sci Total Environ 649:1620–1635. https://doi.org/10.1016/j.scitotenv.2018.08.385

Attermeyer K, Catalán N, Einarsdottir K, et al (2018) Organic Carbon Processing During Transport Through Boreal Inland Waters: Particles as Important Sites. J Geophys Res Biogeosciences 123:2412–2428. https://doi.org/10.1029/2018jg004500

Aufdenkampe AK, Hedges JI, Richey JE, et al (2001) Sorptive fractionation of dissolved organic nitrogen and amino acids onto fine sediments within the Amazon Basin. Limnol Oceanogr 46:1921–1935. https://doi.org/10.4319/lo.2001.46.8.1921

Berthelot H, Duhamel S, L'Helguen S, et al (2019) NanoSIMS single cell analyses reveal the contrasting nitrogen sources for small phytoplankton. Isme J 13:651–662. https://doi.org/10.1038/s41396-018-0285-8

Brailsford FL, Glanville HC, Golyshin PN, et al (2019a) Nutrient enrichment induces a shift in dissolved organic carbon (DOC) metabolism in oligotrophic freshwater sediments. Sci Total Environ 690:1131–1139. https://doi.org/10.1016/j.scitotenv.2019.07.054

Brailsford FL, Glanville HC, Golyshin PN, et al (2019b) Microbial uptake kinetics of dissolved organic carbon (DOC) compound groups from river water and sediments. Sci Rep-uk 9:11229. https://doi.org/10.1038/s41598-019-47749-6

Bull ID, Parekh NR, Hall GH, et al (2000) Detection and classification of atmospheric methane oxidizing bacteria in soil. Nature 405:175–178. https://doi.org/10.1038/35012061

Bunch ND, Bernot MJ (2012) Nitrate and ammonium uptake by natural stream sediment microbial communities in response to nutrient enrichment. Res Microbiol 163:137–141. https://doi.org/10.1016/j.resmic.2011.11.004

568 Burdon FJ, Bai Y, Reyes M, et al (2020) Stream microbial communities and ecosystem
569 functioning show complex responses to multiple stressors in wastewater. Global Change
570 Biol. https://doi.org/10.1111/gcb.15302

571 Callahan BJ, McMurdie PJ, Rosen MJ, et al (2016) DADA2: High-resolution sample inference
572 from Illumina amplicon data. Nat Methods 13:581–583.
573 https://doi.org/10.1038/nmeth.3869

574 Caspi R, Billington R, Keseler IM, et al (2019) The MetaCyc database of metabolic pathways
575 and enzymes—a 2019 update. Nucleic Acids Res 48:D445–D453.
576 https://doi.org/10.1093/nar/gkz862

577 Charteris AF, Knowles TDJ, Michaelides K, Evershed RP (2016) Compound-specific amino
578 acid 15N stable isotope probing of nitrogen assimilation by the soil microbial biomass
579 using gas chromatography/combustion/isotope ratio mass spectrometry. Rapid Commun
580 Mass Sp 30:1846–1856. https://doi.org/10.1002/rcm.7612

581 Chen Y, Murrell JC (2010) When metagenomics meets stable-isotope probing: progress and
582 perspectives. Trends Microbiol 18:157–163. https://doi.org/10.1016/j.tim.2010.02.002

583 Chonova T, Labanowski J, Cournoyer B, et al (2018) River biofilm community changes related
584 to pharmaceutical loads emitted by a wastewater treatment plant. Environ Sci Pollut R
585 25:9254–9264. https://doi.org/10.1007/s11356-017-0024-0

586 Conley M, Mojica M, Mohammed F, et al (2017) Reaction of glycine with glyoxylate:
587 Competing transaminations, aldol reactions, and decarboxylations. J Phys Org Chem
588 30:e3709. https://doi.org/10.1002/poc.3709

589 Coplen TB (2011) Guidelines and recommended terms for expression of stable-isotope-ratio
590 and gas-ratio measurement results. Rapid Commun Mass Sp 25:2538–2560.
591 https://doi.org/10.1002/rcm.5129

592 Costanzo SD, Udy J, Longstaff B, Jones A (2005) Using nitrogen stable isotope ratios (δ15N)
593 of macroalgae to determine the effectiveness of sewage upgrades: changes in the extent
594 of sewage plumes over four years in Moreton Bay, Australia. Mar Pollut Bull 51:212–217.
595 https://doi.org/10.1016/j.marpolbul.2004.10.018

596 Cowie GL, Hedges JI (1994) Biochemical indicators of diagenetic alteration in natural organic
597 matter mixtures. Nature 369:304–307. https://doi.org/10.1038/369304a0

598 Craig H (1957) Isotopic standards for carbon and oxygen and correction factors for mass-
599 spectrometric analysis of carbon dioxide. Geochim Cosmochim Ac 12:133–149.
600 https://doi.org/10.1016/0016-7037(57)90024-8

601 Crump B, Baross J, Simenstad C (1998) Dominance of particle-attached bacteria in the
602 Columbia River estuary, USA. Aquat Microb Ecol 14:7–18.
603 https://doi.org/10.3354/ame014007

Csonka LN, Leisinger T (2007) Biosynthesis of Proline. Ecosal Plus 2:. https://doi.org/10.1128/ecosalplus.3.6.1.4

Dai J, Tang X, Gao G, et al (2013) Effects of salinity and nutrients on sedimentary bacterial communities in oligosaline Lake Bosten, northwestern China. Aquat Microb Ecol 69:123–134. https://doi.org/10.3354/ame01627

Dauwe B, Middelburg JJ (1998) Amino acids and hexosamines as indicators of organic matter degradation state in North Sea sediments. Limnol Oceanogr 43:782–798. https://doi.org/10.4319/lo.1998.43.5.0782

Dekas AE, Parada AE, Mayali X, et al (2019) Characterizing Chemoautotrophy and Heterotrophy in Marine Archaea and Bacteria With Single-Cell Multi-isotope NanoSIP. Front Microbiol 10:2682. https://doi.org/10.3389/fmicb.2019.02682

Docherty G, Jones V, Evershed RP (2001) Practical and theoretical considerations in the gas chromatography/combustion/isotope ratio mass spectrometry δ13C analysis of small polyfunctional compounds. Rapid Commun Mass Sp 15:730–738. https://doi.org/10.1002/rcm.270

Dortch Q (1990) The interaction between ammonium and nitrate uptake in phytoplankton. Mar Ecol Prog Ser 61:183–201. https://doi.org/10.3354/meps061183

Drake TW, Raymond PA, Spencer RGM (2018) Terrestrial carbon inputs to inland waters: A current synthesis of estimates and uncertainty. Limnology Oceanogr Lett 3:132–142. https://doi.org/10.1002/lol2.10055

Drury B, Rosi-Marshall E, Kelly JJ (2013) Wastewater Treatment Effluent Reduces the Abundance and Diversity of Benthic Bacterial Communities in Urban and Suburban Rivers. Appl Environ Microb 79:1897–1905. https://doi.org/10.1128/aem.03527-12

Du Y, Ramirez CE, Jaffé R (2018) Fractionation of Dissolved Organic Matter by Co-Precipitation with Iron: Effects of Composition. Environ Process 5:5–21. https://doi.org/10.1007/s40710-017-0281-4

Dugdale RC, Goering JJ (1967) UPTAKE OF NEW AND REGENERATED FORMS OF NITROGEN IN PRIMARY PRODUCTIVITY1: UPTAKE OF NITROGEN IN PRIMARY PRODUCTIVITY. Limnol Oceanogr 12:196–206. https://doi.org/10.4319/lo.1967.12.2.0196

Einarsdóttir K, Attermeyer K, Hawkes JA, et al (2020) Particles and Aeration at Mire-Stream Interfaces Cause Selective Removal and Modification of Dissolved Organic Matter. J Geophys Res Biogeosciences 125:. https://doi.org/10.1029/2020jg005654

Evans CD, Monteith DT, Cooper DM (2005) Long-term increases in surface water dissolved organic carbon: Observations, possible causes and environmental impacts. Environ Pollut 137:55–71. https://doi.org/10.1016/j.envpol.2004.12.031

639 Evershed RP, Crossman ZM, Bull ID, et al (2006) 13C-Labelling of lipids to investigate
640 microbial communities in the environment. Curr Opin Biotech 17:72–82.
641 https://doi.org/10.1016/j.copbio.2006.01.003

642 Fernandes D, Wu Y, Shirodkar PV, et al (2020) Sources and preservation dynamics of organic
643 matter in surface sediments of Narmada River, India – Illustrated by amino acids. J
644 Marine Syst 201:103239. https://doi.org/10.1016/j.jmarsys.2019.103239

645 Fernandes D, Wu Y, Shirodkar PV, et al (2019) Spatial and temporal variations in source,
646 diagenesis, and fate of organic matter in sediments of the Netravati River, India. Hydrol
647 Process 33:2642–2657. https://doi.org/10.1002/hyp.13516

648 Fichman Y, Gerdes SY, Kovács H, et al (2015) Evolution of proline biosynthesis: enzymology,
649 bioinformatics, genetics, and transcriptional regulation. Biol Rev 90:1065–1099.
650 https://doi.org/10.1111/brv.12146

651 Glibert PM, Heil CA, Madden CJ, Kelly SP (2021) Dissolved organic nutrients at the interface
652 of fresh and marine waters: flow regime changes, biogeochemical cascades and
653 picocyanobacterial blooms—the example of Florida Bay, USA. Biogeochemistry 1–27.
654 https://doi.org/10.1007/s10533-021-00760-4

655 Glibert PM, Middelburg JJ, McClelland JW, Zanden MJV (2019) Stable isotope tracers:
656 Enriching our perspectives and questions on sources, fates, rates, and pathways of major
657 elements in aquatic systems. Limnol Oceanogr 64:950–981.
658 https://doi.org/10.1002/lno.11087

659 Glibert PM, Wilkerson FP, Dugdale RC, et al (2016) Pluses and minuses of ammonium and
660 nitrate uptake and assimilation by phytoplankton and implications for productivity and
661 community composition, with emphasis on nitrogen-enriched conditions. Limnol
662 Oceanogr 61:165–197. https://doi.org/10.1002/lno.10203

663 Groeneveld M, Catalán N, Attermeyer K, et al (2020) Selective Adsorption of Terrestrial
664 Dissolved Organic Matter to Inorganic Surfaces Along a Boreal Inland Water Continuum. J
665 Geophys Res Biogeosciences 125:. https://doi.org/10.1029/2019jg005236

666 GUPTA LP, SUBRAMANIAN V, ITTEKKOT V (1997) Biogeochemistry of particulate organic
667 matter transported by the Godavari River, India. Biogeochemistry 38:103–128.
668 https://doi.org/10.1023/a:1005732519216

669 Gweon HS, Bowes MJ, Moorhouse HL, et al (2021) Contrasting community assembly
670 processes structure lotic bacteria metacommunities along the river continuum. Environ
671 Microbiol 23:484–498. https://doi.org/10.1111/1462-2920.15337

672 Hagberg A, Gupta S, Rzhepishevska O, et al (2021) Do environmental pharmaceuticals affect
673 the composition of bacterial communities in a freshwater stream? A case study of the
674 Knivsta river in the south of Sweden. Sci Total Environ 763:142991.
675 https://doi.org/10.1016/j.scitotenv.2020.142991

676 He W, Chen M, Schlautman MA, Hur J (2016) Dynamic exchanges between DOM and POM
677 pools in coastal and inland aquatic ecosystems: A review. Sci Total Environ 551:415–428.
678 https://doi.org/10.1016/j.scitotenv.2016.02.031

679 Jia Z, Liu T, Xia X, Xia N (2016) Effect of particle size and composition of suspended sediment
680 on denitrification in river water. Sci Total Environ 541:934–940.
681 https://doi.org/10.1016/j.scitotenv.2015.10.012

682 Junk G, Svec HJ (1958) The absolute abundance of the nitrogen isotopes in the atmosphere
683 and compressed gas from various sources. Geochim Cosmochim Ac 14:234–243.
684 https://doi.org/10.1016/0016-7037(58)90082-6

685 Kerner M, Hohenberg H, Ertl S, et al (2003) Self-organization of dissolved organic matter to
686 micelle-like microparticles in river water. Nature 422:150–154.
687 https://doi.org/10.1038/nature01469

688 Knowles TDJ, Chadwick DR, Bol R, Evershed RP (2010) Tracing the rate and extent of N and C
689 flow from 13C,15N-glycine and glutamate into individual de novo synthesised soil amino
690 acids. Org Geochem 41:1259–1268. https://doi.org/10.1016/j.orggeochem.2010.09.003

691 Lu Y, Bauer JE, Canuel EA, et al (2013) Photochemical and microbial alteration of dissolved
692 organic matter in temperate headwater streams associated with different land use. J
693 Geophys Res Biogeosciences 118:566–580. https://doi.org/10.1002/jgrg.20048

694 Mackay EB, Feuchtmayr H, Ville MMD, et al (2020) Dissolved organic nutrient uptake by
695 riverine phytoplankton varies along a gradient of nutrient enrichment. Sci Total Environ
696 722:137837. https://doi.org/10.1016/j.scitotenv.2020.137837

697 Manefield M, Whiteley AS, Griffiths RI, Bailey MJ (2002) RNA Stable Isotope Probing, a Novel
698 Means of Linking Microbial Community Function to Phylogeny. Appl Environ Microb
699 68:5367–5373. https://doi.org/10.1128/aem.68.11.5367-5373.2002

700 Mansour I, Heppell CM, Ryo M, Rillig MC (2018) Application of the microbial community
701 coalescence concept to riverine networks. Biol Rev 93:1832–1845.
702 https://doi.org/10.1111/brv.12422

703 Martin M (2011) Cutadapt removes adapter sequences from high-throughput sequencing
704 reads. Embnet J 17:10–12. https://doi.org/10.14806/ej.17.1.200

705 Mayer LM, Schick LL, Skorko K, Boss E (2006) Photodissolution of particulate organic matter
706 from sediments. Limnol Oceanogr 51:1064–1071.
707 https://doi.org/10.4319/lo.2006.51.2.1064

708 Meija J, Coplen TB, Berglund M, et al (2016) Isotopic compositions of the elements 2013
709 (IUPAC Technical Report). Pure Appl Chem 88:293–306. https://doi.org/10.1515/pac-
710 2015-0503

711 Middelburg J, Nieuwenhuize J (2000) Nitrogen uptake by heterotrophic bacteria and
712 phytoplankton in the nitrate-rich Thames estuary. Mar Ecol Prog Ser 203:13–21.
713 https://doi.org/10.3354/meps203013

714 Monteith DT, Stoddard JL, Evans CD, et al (2007) Dissolved organic carbon trends resulting
715 from changes in atmospheric deposition chemistry. Nature 450:537–540.
716 https://doi.org/10.1038/nature06316

717 Morgan M, Anders S, Lawrence M, et al (2009) ShortRead: a bioconductor package for input,
718 quality assessment and exploration of high-throughput sequence data. Bioinformatics
719 25:2607–2608. https://doi.org/10.1093/bioinformatics/btp450

720 Müller G, Middelburg JJ, Sluijs A (2021) Introducing GloRiSe – a global database on river
721 sediment composition. Earth Syst Sci Data 13:3565–3575. https://doi.org/10.5194/essd-
722 13-3565-2021

723 Nemergut DR, Schmidt SK, Fukami T, et al (2013) Patterns and Processes of Microbial
724 Community Assembly. Microbiol Mol Biol R 77:342–356.
725 https://doi.org/10.1128/mmbr.00051-12

726 Noacco V, Duffy CJ, Wagener T, et al (2019) Drivers of interannual and intra-annual
727 variability of dissolved organic carbon concentration in the River Thames between 1884
728 and 2013. Hydrol Process 33:994–1012. https://doi.org/10.1002/hyp.13379

729 Pemberton JA, Lloyd CEM, Arthur CJ, et al (2020) Untargeted characterisation of dissolved
730 organic matter contributions to rivers from anthropogenic point sources using direct-
731 infusion and high-performance liquid chromatography/Orbitrap mass spectrometry.
732 Rapid Commun Mass Sp 34:. https://doi.org/10.1002/rcm.8618

733 Phillips JM, Russell MA, Walling DE (2000) Time-integrated sampling of fluvial suspended
734 sediment: a simple methodology for small catchments. Hydrol Process 14:2589–2602.
735 https://doi.org/10.1002/1099-1085(20001015)14:14<2589::aid-hyp94>3.3.co;2-4

736 Quast C, Pruesse E, Yilmaz P, et al (2013) The SILVA ribosomal RNA gene database project:
737 improved data processing and web-based tools. Nucleic Acids Res 41:D590–D596.
738 https://doi.org/10.1093/nar/gks1219

739 Reay MK, Charteris AF, Jones DL, Evershed RP (2019) 15N-amino sugar stable isotope
740 probing (15N-SIP) to trace the assimilation of fertiliser-N by soil bacterial and fungal
741 communities. Soil Biology Biochem 138:107599.
742 https://doi.org/10.1016/j.soilbio.2019.107599

743 Regnier P, Friedlingstein P, Ciais P, et al (2013) Anthropogenic perturbation of the carbon
744 fluxes from land to ocean. Nat Geosci 6:597–607. https://doi.org/10.1038/ngeo1830

745 Reitzer L (2004) Biosynthesis of Glutamate, Aspartate, Asparagine, L -Alanine, and D -
746 Alanine. Ecosal Plus 1:. https://doi.org/10.1128/ecosalplus.3.6.1.3

747 Sánchez-Carrillo S, Álvarez-Cobelas M (2018) Stable isotopes as tracers in aquatic
748 ecosystems. Environ Rev 26:69–81. https://doi.org/10.1139/er-2017-0040

749 Simon M, Grossart H, Schweitzer B, Ploug H (2002) Microbial ecology of organic aggregates
750 in aquatic ecosystems. Aquat Microb Ecol 28:175–211.
751 https://doi.org/10.3354/ame028175

752 Smith MW, Allen LZ, Allen AE, et al (2013) Contrasting genomic properties of free-living and
753 particle-attached microbial assemblages within a coastal ecosystem. Front Microbiol
754 4:120. https://doi.org/10.3389/fmicb.2013.00120

755 Stauffer GV (2004) Regulation of Serine, Glycine, and One-Carbon Biosynthesis. Ecosal Plus
756 1:. https://doi.org/10.1128/ecosalplus.3.6.1.2

757 Steffy LY, Kilham SS (2004) ELEVATED δ15N IN STREAM BIOTA IN AREAS WITH SEPTIC TANK
758 SYSTEMS IN AN URBAN WATERSHED. Ecol Appl 14:637–641. https://doi.org/10.1890/03-
759 5148

760 Stein LY, Klotz MG (2016) The nitrogen cycle. Curr Biol 26:R94–R98.
761 https://doi.org/10.1016/j.cub.2015.12.021

762 Veuger B, Middelburg JJ, Boschker HTS, Houtekamer M (2005) Analysis of 15N incorporation
763 into D-alanine: A new method for tracing nitrogen uptake by bacteria. Limnology
764 Oceanogr Methods 3:230–240. https://doi.org/10.4319/lom.2005.3.230

765 Walters W, Hyde ER, Berg-Lyons D, et al (2016) Improved Bacterial 16S rRNA Gene (V4 and
766 V4-5) and Fungal Internal Transcribed Spacer Marker Gene Primers for Microbial
767 Community Surveys. Msystems 1:e00009-15. https://doi.org/10.1128/msystems.00009-
768 15

769 Wang L, Zhang J, Li H, et al (2018) Shift in the microbial community composition of surface
770 water and sediment along an urban river. Sci Total Environ 627:600–612.
771 https://doi.org/10.1016/j.scitotenv.2018.01.203

772 Wang Y, Huang WE, Cui L, Wagner M (2016) Single cell stable isotope probing in
773 microbiology using Raman microspectroscopy. Curr Opin Biotech 41:34–42.
774 https://doi.org/10.1016/j.copbio.2016.04.018

775 Wu L, Ning D, Zhang B, et al (2019) Global diversity and biogeography of bacterial
776 communities in wastewater treatment plants. Nat Microbiol 4:1183–1195.
777 https://doi.org/10.1038/s41564-019-0426-5

778 Xia X, Liu T, Yang Z, et al (2017) Enhanced nitrogen loss from rivers through coupled
779 nitrification-denitrification caused by suspended sediment. Sci Total Environ 579:47–59.
780 https://doi.org/10.1016/j.scitotenv.2016.10.181

781 Yamashita Y, Jaffé R (2008) Characterizing the Interactions between Trace Metals and
782 Dissolved Organic Matter Using Excitation−Emission Matrix and Parallel Factor Analysis.
783 Environ Sci Technol 42:7374–7379. https://doi.org/10.1021/es801357h

784 Yates CA, Johnes PJ, Spencer RGM (2016) Assessing the drivers of dissolved organic matter
785 export from two contrasting lowland catchments, U.K. Sci Total Environ 569:1330–1340.
786 https://doi.org/10.1016/j.scitotenv.2016.06.211

787 Yates CA, Johnes PJ, Spencer RGM (2019) Characterisation of treated effluent from four
788 commonly employed wastewater treatment facilities: A UK case study. J Environ Manage
789 232:919–927. https://doi.org/10.1016/j.jenvman.2018.12.006

790 Yoshimura C, Fujii M, Omura T, Tockner K (2010) Instream release of dissolved organic
791 matter from coarse and fine particulate organic matter of different origins.
792 Biogeochemistry 100:151–165. https://doi.org/10.1007/s10533-010-9412-y

793 Zeglin LH (2015) Stream microbial diversity in response to environmental changes: review
794 and synthesis of existing research. Front Microbiol 6:454.
795 https://doi.org/10.3389/fmicb.2015.00454

796 Zhang X, Ward BB, Sigman DM (2020) Global Nitrogen Cycle: Critical Enzymes, Organisms,
797 and Processes for Nitrogen Budgets and Dynamics. Chem Rev 120:5308–5351.
798 https://doi.org/10.1021/acs.chemrev.9b00613

799 Pinheiro J, Bates D, DebRoy S, Sarkar D, R Core Team (2021). nlme: Linear and Nonlinear
800 Mixed Effects Models. R package version 3.1-148, https://CRAN.R-
801 project.org/package=nlme

802 Pagès H, Aboyoun P, Gentleman R, DebRoy S (2021). Biostrings: Efficient manipulation of
803 biological strings. R package version 2.60.1,
804 https://bioconductor.org/packages/Biostrings

805 R Core Team (2021). R: A language and environment for statistical computing. R Foundation
806 for Statistical Computing, Vienna, Austria. URL https://www.R-project.org/

807 **List of figures**

814 Glx (B) and Pro (C). Dash lines show regression models during the first 24 h of the
815 experiment.
816 **Fig. 4** Average percentage of assimilation of ^{15}N-nitrate into individual proteinaceous AAs
817 over time. Error bars show the *SE* (*n* = 6).
818 **Fig. 5** Rates and percentages of assimilation of ^{15}N and ^{13}C from Glu (A and B, respectively)
819 and ^{15}N-nitrate (C) into individual proteinaceous AAs. The circle represents the average
820 composition of the pool of THAAs in mol %. The colour of the arrows represents the specific
821 assimilation rates (*V*, h^{-1}) after 3 h, the width is proportional to the percentage of
822 assimilation of the substrate after 72 h, and the direction represents the transfer of C or N
823 according to the primary biosynthetic pathways of each AA (D).
824 **Fig. 6** Percentage of assimilation of ^{13}C and ^{15}N into the pool of THAAs over time (A), and the
825 spatial differences in assimilation after 72 h (B). Error bars show the *SE* (*n* = 6) (A).

Figures

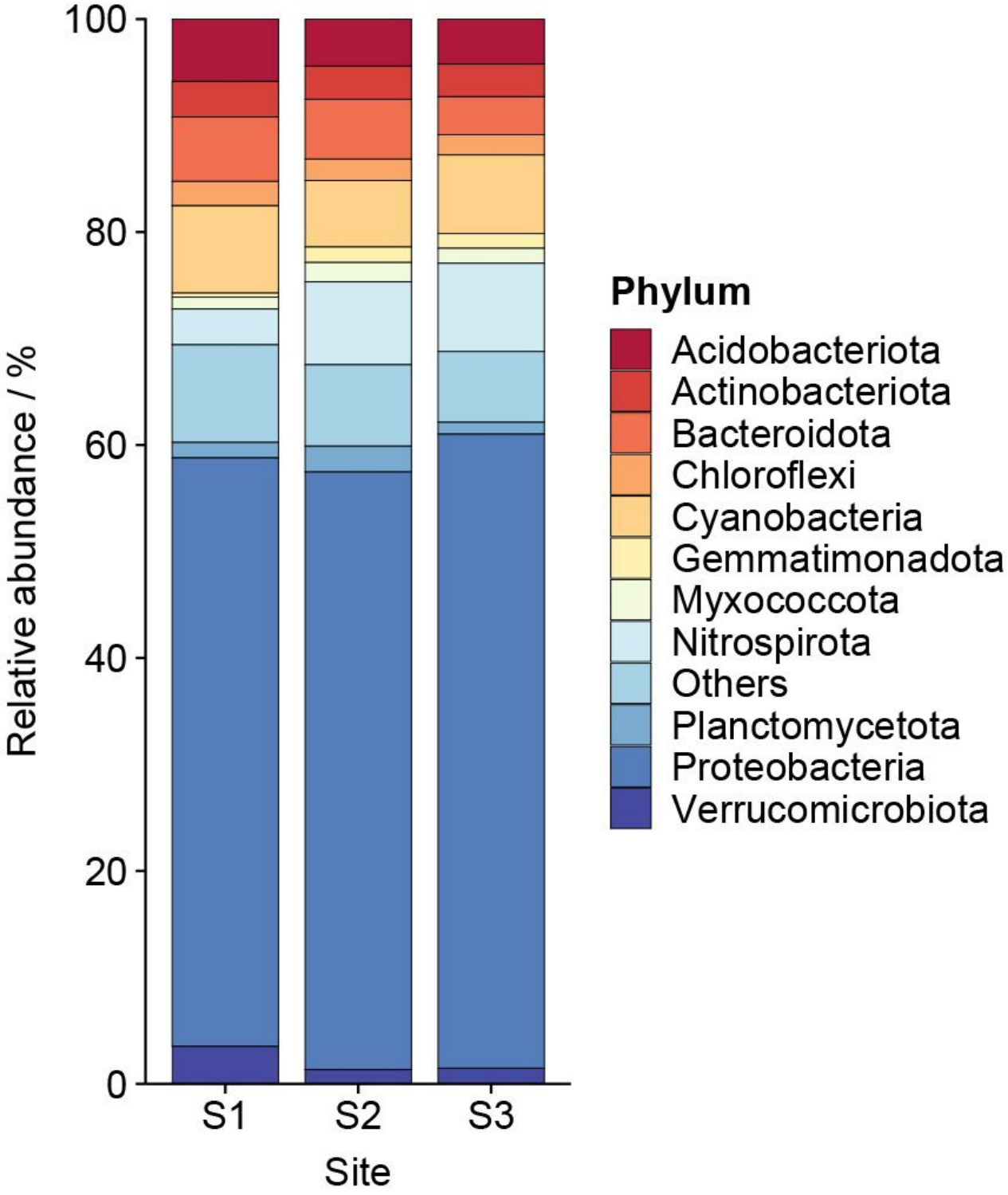

Figure 1

Phylum level bacterial community composition in suspended POM in the River Chew, UK based on 16S rRNA gene sequencing.

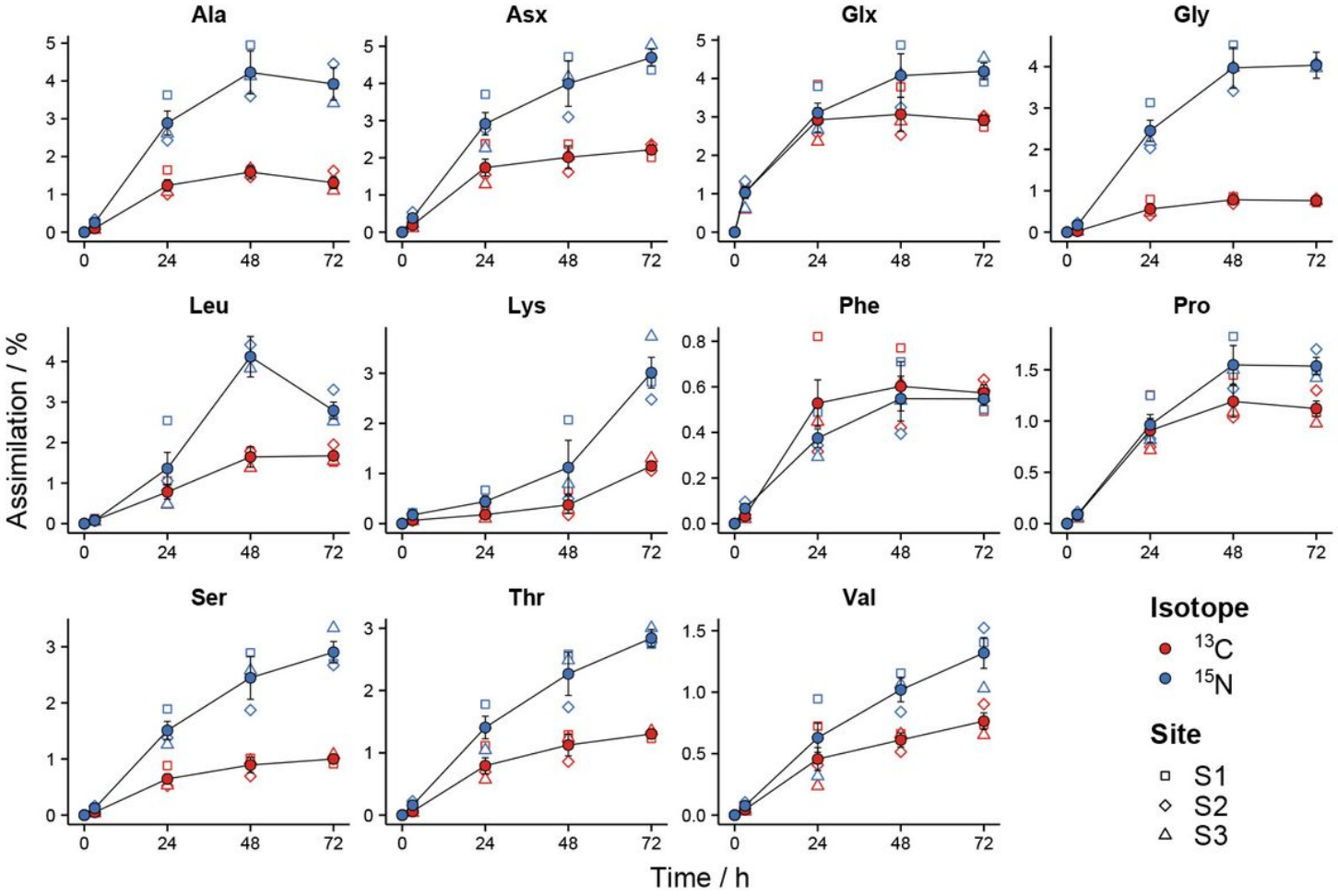

Figure 2

Average percentage of assimilation of 13C,15N-Glu into individual proteinaceous AAs over time. Error bars show the SE (n = 6).

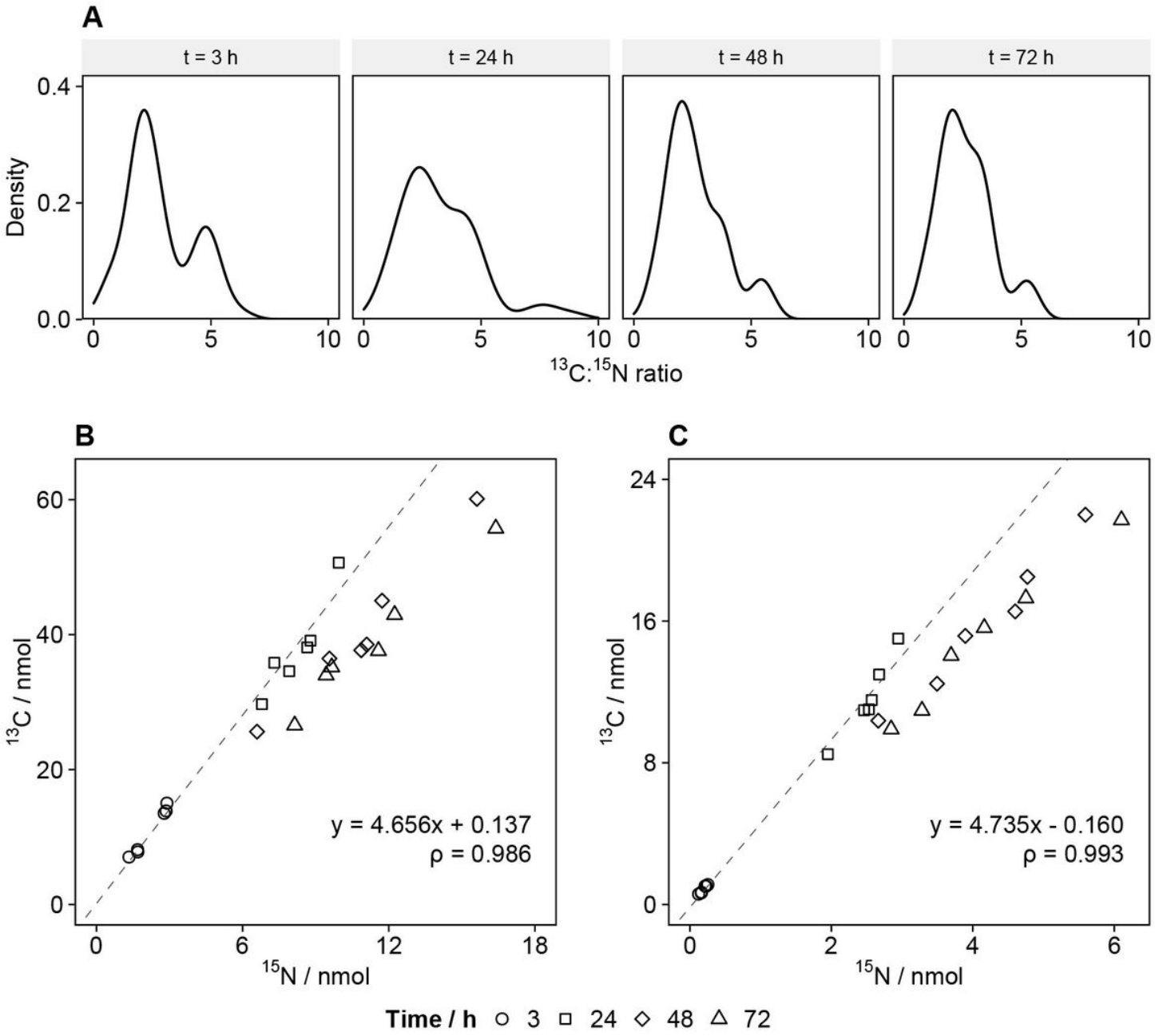

Figure 3

Density distribution of the 13C:15N ratio of individual proteinaceous AAs at different time points following the addition of 13C,15N-Glu (A). Relationship of 13C to 15N over time for Glx (B) and Pro (C). Dash lines show regression models during the first 24 h of the experiment.

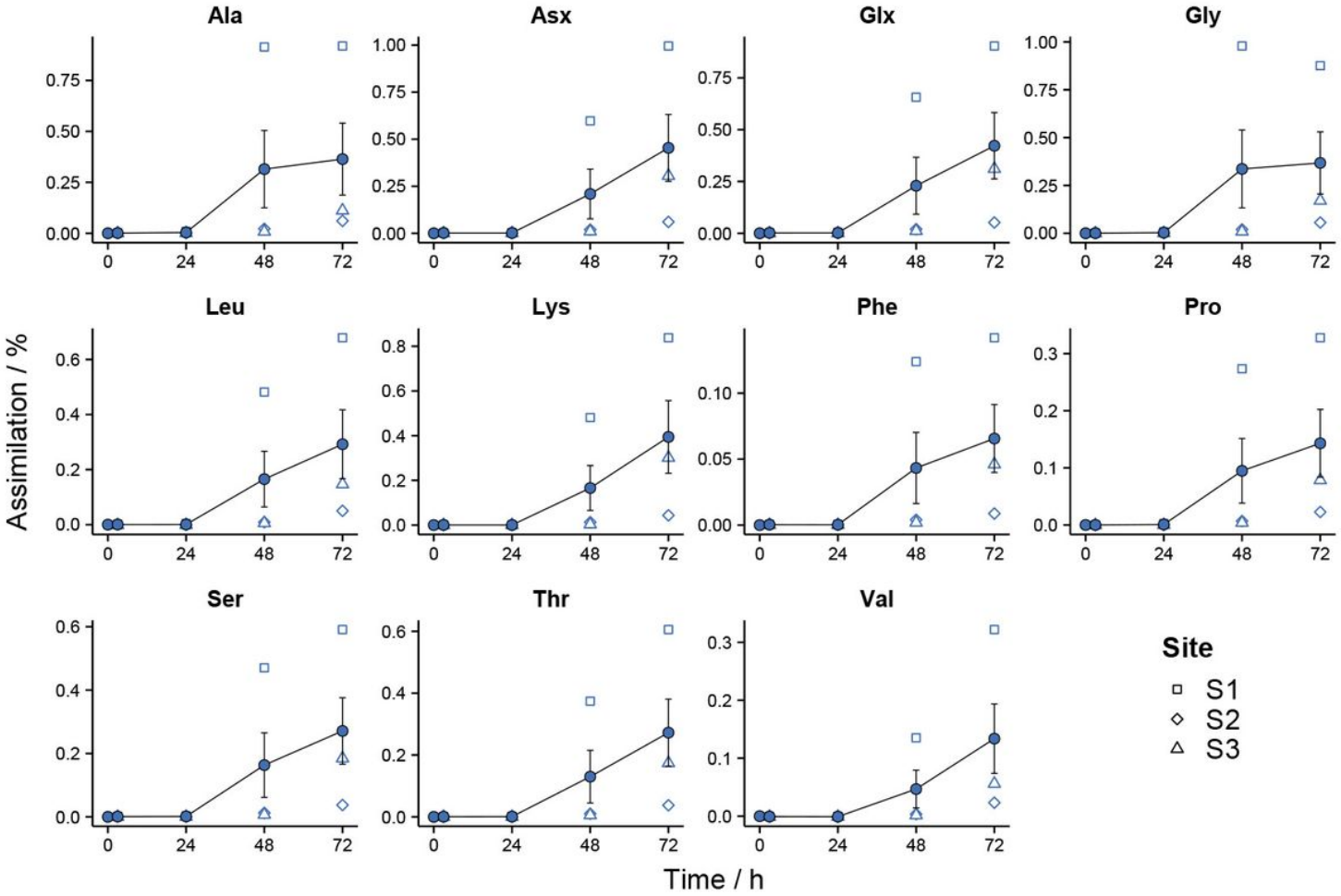

Figure 4

Average percentage of assimilation of 15N-nitrate into individual proteinaceous AAs over time. Error bars show the SE (n = 6).

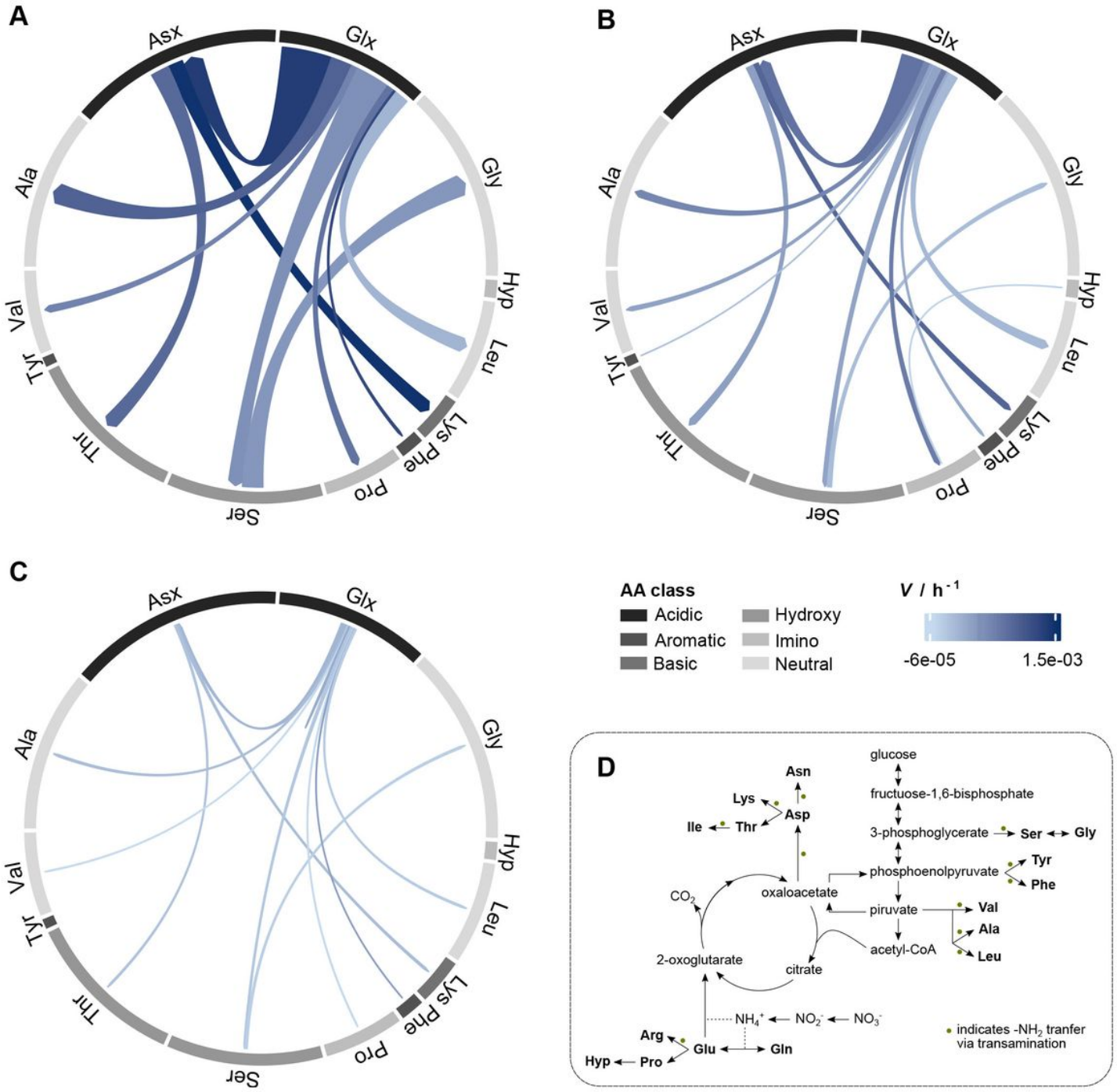

Figure 5

Rates and percentages of assimilation of 15N and 13C from Glu (A and B, respectively) and 15N-nitrate (C) into individual proteinaceous AAs. The circle represents the average composition of the pool of THAAs in mol %. The colour of the arrows represents the specific assimilation rates (V, h-1) after 3 h, the width is proportional to the percentage of assimilation of the substrate after 72 h, and the direction represents the transfer of C or N according to the primary biosynthetic pathways of each AA (D).

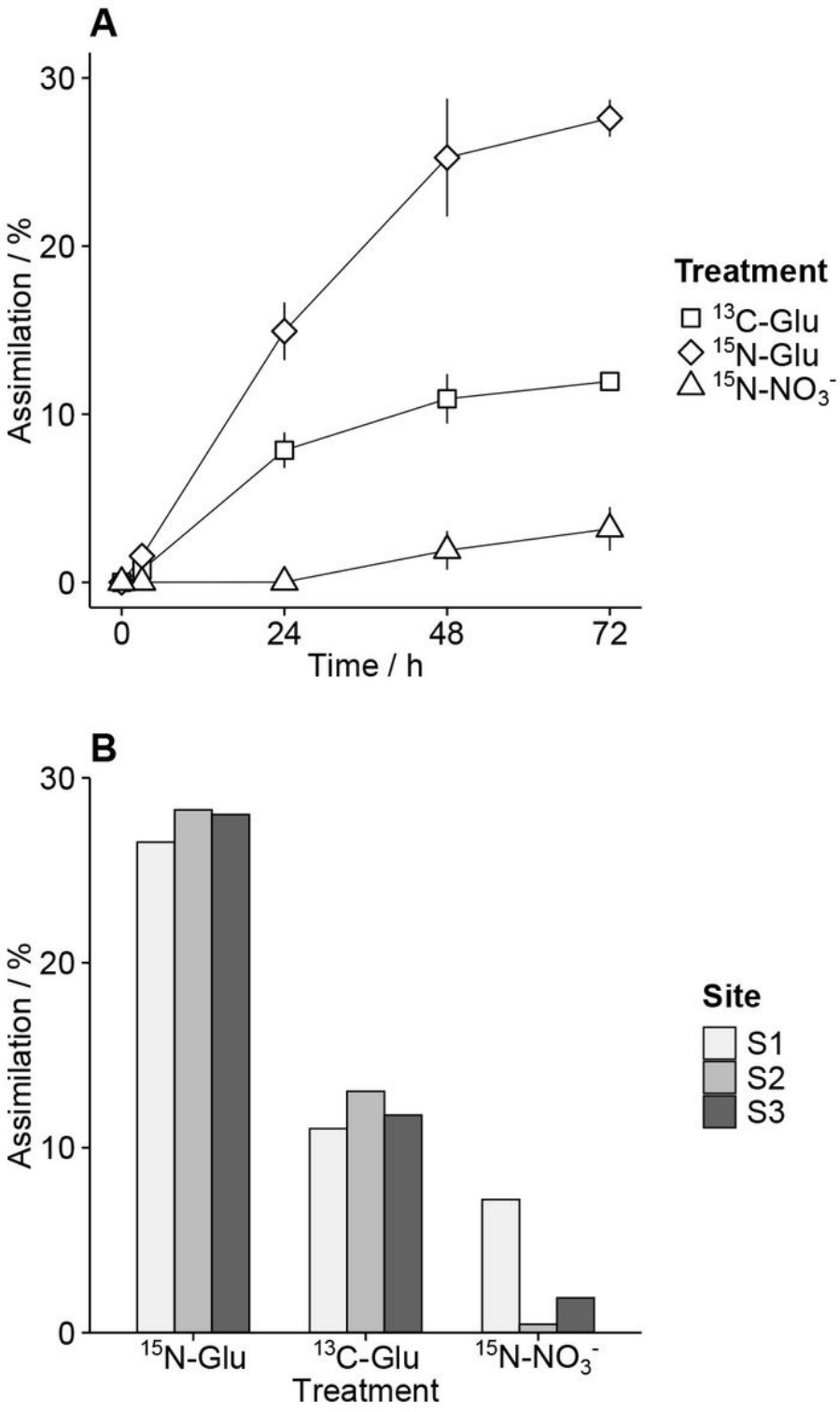

Figure 6

Percentage of assimilation of 13C and 15N into the pool of THAAs over time (A), and the spatial differences in assimilation after 72 h (B). Error bars show the SE (n = 6) (A).

Supplementary Files

This is a list of supplementary files associated with this preprint. Click to download.

- Supplementaryinformation.docx